ARTICLE

A power spectrum approach to tally convergence in Monte Carlo criticality calculation

Taro Ueki*†

Japan Atomic Energy Agency, Nuclear Safety Research Center,

Fuel Cycle Safety Research Division, Criticality Safety Research Group.

Abstract

In Monte Carlo criticality calculation, confidence interval estimation is based on the central limit theorem (CLT) for a series of tallies from generations in equilibrium. A fundamental assertion resulting from CLT is the convergence in distribution (CID) of the interpolated standardized time series (ISTS) of tallies. In this work, the spectral analysis of ISTS has been conducted in order to assess the convergence of tallies in terms of CID. Numerical results obtained indicate that the power spectrum of ISTS is equal to the theoretically predicted power spectrum of Brownian motion for tallies of effective neutron multiplication factor; on the other hand, the power spectrum of ISTS of a strongly correlated series of tallies from local powers fluctuates wildly while maintaining the spectral form of fractional Brownian motion. The latter result is the evidence of a case where a series of tallies is away from CID, while the spectral form supports normality assumption on the sample mean. It is also demonstrated that one can make the unbiased estimation of the standard deviation of sample mean well before CID occurs.

Keywords; Monte Carlo criticality, power spectrum, convergence in distribution

"This is an accepted manuscript of an article published by Taylor & Francis in Journal of Nuclear Science and Technology on December 2017, available at https://doi.org/10.1080/00223131.2017.1365022."

* Email: ueki.taro@jaea.go.jp

† Address: 2-4 Shirakata-Shirane, Tokai-Mura, Naka-Gun, Ibaraki-Ken 319-1195, Japan

1. Introduction

Monte Carlo (MC) codes with neutron transport capabilities [1,2,3] are important analysis tools in the nuclear energy fields. In these MC codes, effective neutron multiplication factor (k_{eff}) and its perturbation, power distribution, and kinetic parameters are computed by the criticality mode where a fission source generation in equilibrium is iterated to yield a series of tallies. These iterations are of a form of the power method with particle population normalization [4]. Consequently, the sources in adjacent generations are dependent and a series of tallies is under correlation. A significant amount of research has been conducted on the standard deviation estimation of the sample mean of tallies [5-10]. Many estimators were investigated by incorporating or excluding the influence of correlation. However, assessment in terms of the weak convergence in the central limit theorem (CLT) has not been explicitly conducted. For this reason, it is worthwhile investigating the convergence of the sample mean of tallies by way of spectral analysis, since the weak convergence in CLT is equivalent to convergence in distribution (CID). In this work, power spectrum is computed for a series of tallies and compared with a reference spectrum from Brownian motion. If contrasted with the spectral analysis approach to MC fission source distribution [11], the computation of power spectrum and the availability of reference stochastic processes such as Brownian motion and Brownian bridge are unique and novel aspects in this work. The essential element of spectral analysis in this work is an interpolated standardized time series (ISTS) which was originally introduced in MC criticality calculation in some previous investigation of statistical error estimation [12]. The ISTS methodology is itself based on theoretical developments by operations research scientists [13,14]. Numerical results are demonstrated for models of PWR initial core [15] and UO_2-concrete debris [16].

The variance of the sample mean of tallies is the lag zero autocovariance, i.e., the variance of tally at a generation, plus twice the sum of autocovariances through lags, divided by the number of generations iterated [17]. In this respect, if there exists a method for

accurately estimating individual autocovariances, one can in principle compute the standard deviation of sample mean in an unbiased manner. However, these autocovariances are reliably estimated only for small lags. In addition, if a series of tallies are under strong positive correlation, the estimates of autocovariances over adjacent lags tend to be under strong positive correlation, which leads to the large uncertainty of the sum through lags. Even negative estimates can arise if the sum is not artificially truncated [8]. Motivated by these challenges, the computation of the standard deviation of the sample mean of tallies has been an actively investigated topic since the implementation of non-overlapping batch means (NBM) by Gelbard and Prael [5]. In this work, CID is argued much more explicitly than any of previous works [5-10]. A pre-CID phenomenon is also investigated where the inverse square-root law of decrease appears during insufficient-CID generations.

This paper is organized as follows. In Section 2, the CLT for a correlated series is reviewed together with Brownian motion, Brownian bridge, and ISTS. In Section 3, fractional Brownian motion (FBM) is introduced as a generalization of Brownian motion. The analysis of power spectrum is then proposed as a theoretically founded tally convergence assessment tool alternative to the ad-hoc run length diagnosis with fractal dimension [18]. The use of power spectrum is also argued for identifying the pre-CID phenomenon. Sections 4 and 5 demonstrate the power spectrum of ISTS for models of PWR initial core and UO_2-concrete debris, respectively, together with the standard deviation estimation of sample mean. In Section 6, milestones achieved are summarized together with an issue for future work.

2. Central Limit Theorem (CLT) and Standardized Time Series

In MC criticality calculation, a fission source generation in equilibrium is stochastically iterated in a form of the power method with particle population normalization. Consequently, the generations yield a correlated series of tallies denoted as $x_1, x_2, \ldots, x_n$ for which the joint statistical property of x_j and x_k is the same as that of x_{j+m} and x_{k+m}, i.e., translation invariant with respect to generation shift. Here the subscript denotes the generation number in

equilibrium and the largest subscript n is the total number of generations iterated through equilibrium. The tally x is estimated by the sample mean of $x_1, x_2, \ldots, x_n$ and the variance of the sample mean is

$$\frac{1}{n}\left[AC(0) + 2\sum_{j=1}^{n-1}\left(1-\frac{j}{n}\right)AC(j) \right] \tag{1}$$

where Σ is the symbol for summation, $AC(j)$ is the lag j autocovariance of x_i and x_{i+j} [17]. When the total number of generations is sufficiently large, Eq (1) becomes

$$\frac{1}{n}\left[AC(0) + 2\sum_{j=1}^{n-1}\left(1-\frac{j}{n}\right)AC(j) \right] \approx \frac{\sigma^2}{n} \equiv \frac{1}{n}\left[AC(0) + 2\sum_{j=1}^{\infty} AC(j) \right]. \tag{2}$$

This approximation is justified as far as n is large enough in terms of the attenuation of $AC(j)$. In this respect, the validity of Eq (2) is not directly influenced by CID. For example, when $AC(j)$ becomes negligibly small in magnitude at about lag 200, n=5000 will be sufficiently large for Eq (2) to be valid. However, n=5000 may not be large enough so as to ensure CID. The possibility of such a case cannot be excluded and will be a topic in numerical computations.

Brownian motion referred to in Section 1 is a vehicle for analyzing the CID of a correlated series of tallies from equilibrium. The path of Brownian motion, if denoted as $B_M(t)$, is known to satisfy [19]:

(BM) (a) For $0 \le t_0 < t_1 < t_2 < \cdots < t_m$, $B_M(t_0)$, $B_M(t_1) - B_M(t_0)$, $B_M(t_2) - B_M(t_1), \cdots,$ $B_M(t_m) - B_M(t_{m-1})$ are independent,

(b) $P_R(B_M(t+h) - B_M(t) \le z) = (2\pi h)^{-1/2} \int_{-\infty}^{z} \exp(-u^2/(2h))du$, $t \ge 0$, $h > 0$,

(c) $P_R(B_M(0) = 0) = 1$ and $B_M(t)$ is continuous with probability 1 for $t \ge 0$,

where P_R stands for probability. Hereafter, citation will be made as (BM), (a) in (BM), etc. To proceed, it is convenient to introduce notations for the mean and the partial sample mean of $x_1, x_2, \ldots, x_n$:

$$\mu \equiv E[x_i], \tag{3}$$

$$s_m \equiv \frac{1}{m}\sum_{i=1}^{m} x_i \ , \ 1 \le m \le n \, , \tag{4}$$

where $E[\ ]$ is the notation for an expected value. The weak convergence in CLT is then stated as [14]

$$\frac{\sum_{i=1}^{\lfloor nt \rfloor} x_i - \lfloor nt \rfloor \mu}{\sigma\sqrt{n}} = \frac{\lfloor nt \rfloor \left(s_{\lfloor nt \rfloor} - \mu \right)}{\sigma\sqrt{n}} \rightarrow_D B_M(t) \quad \text{for } 0 \le t \le 1 \text{ as } n \rightarrow \infty \tag{5}$$

where $\lfloor nt \rfloor$ is the largest integer not exceeding nt and $\rightarrow_D$ stands for CID. Eq (5) asserts that as $n \rightarrow \infty$, the cumulative distribution function (cdf) of $(\sum_{i=1}^{\lfloor nt \rfloor} x_i - \lfloor nt \rfloor \mu)/\sigma\sqrt{n}$ converges to the cdf of $B_M(t)$ for all t in [0,1]. Historically, the CLT for dependent variables was first proved in 1961 [20] and subsequently refined as in the CID in Eq (5) in the fields of operations research [13].

At first glance, Eq (5) appears to suggest the analysis of $(\sum_{i=1}^{\lfloor nt \rfloor} x_i - \lfloor nt \rfloor \mu)/\sqrt{n}$ in order to estimate σ from the amplitude. However, the mean μ is itself one of the quantities to be estimated in MC criticality calculation and the exact value of μ cannot be known. To overcome this dilemma, other theorem was derived and utilized in the communities of simulations and operations research [13,14],

$$T_n(t) \equiv \frac{\lfloor nt \rfloor (s_n - s_{\lfloor nt \rfloor})}{\sigma\sqrt{n}} \rightarrow_D B_B(t) \equiv B_M(t) - tB_M(1) \quad \text{for } 0 \le t \le 1 \text{ as } n \rightarrow \infty, \tag{6}$$

where $T_n(t)$ is the ISTS referred to in Section 1 and $B_B(t)$ is the path of Brownian bridge. Note that the subscripts in the numerator of Eq (6) are n and $\lfloor nt \rfloor$. It is also worth mentioning that $T_n(i/n)$, i=0,…,n, is known as standardized time series. A sketchy derivation of Eq (6) from Eq (5) is also found elsewhere [12]. Unlike the case of Eq (5), it is possible to analyze $\lfloor nt \rfloor (s_n - s_{\lfloor nt \rfloor})/\sqrt{n}$ in Eq (6) in order to obtain an estimate of σ from the amplitude since s_n and $s_{\lfloor nt \rfloor}$ are both computable from a series of tallies. Eqs (5) and (6) imply that the CID toward Brownian motion transforms to the CID toward Brownian bridge if the mean μ is replaced by s_n.

The covariance of Brownian bridge is easily computed using the covariance of Brownian motion $E[B_M(t)B_M(u)] = \min(t,u)$ (from (a) and (b) in (BM)) as

$$E[B_B(t)B_B(u)] = \min(t,u) - tu \quad \text{for} \quad 0 \le t,u \le 1. \tag{7}$$

Based on Eq (7), an estimator of σ^2 can be constructed as follows [12]. First, a family of weighting functions is introduced as

$$w_j^C(t) = \sqrt{8}\pi j \cos(2\pi jt), \quad w_j^S(t) = \sqrt{8}\pi j \sin(2\pi jt), \quad j=1,2,\ldots, \tag{8}$$

for which orthonormality relation holds [12]:

$$\int_0^1 \int_0^1 w_j^F(t) w_k^H(s) E[B_B(t)B_B(s)]dsdt = \delta_{F,H}\delta_{j,k} \quad \text{for } F,H=C,S, \quad j,k=1,2,\ldots. \tag{9}$$

Here δ with two subscripts denotes the Kronecker delta. Second, a statistic is defined as

$$Z_j^F(n) \equiv \frac{1}{n}\sum_{m=1}^{n-1} w_j^F\left(\frac{m}{n}\right)\sigma T_n\left(\frac{m}{n}\right) = \frac{1}{n}\sum_{m=1}^{n-1} w_j^F\left(\frac{m}{n}\right)\frac{m(s_n - s_m)}{\sqrt{n}}, \; F=C,S, \quad j=1,2,\ldots, \tag{10}$$

which satisfies [12]

$$E[Z_j^F(n)Z_k^H(n)] \to \sigma^2\delta_{F,H}\delta_{j,k} \quad \text{for} \quad F,H=C,S, \quad j,k=1,2,\ldots \text{ as } n\to\infty. \tag{11}$$

The variance of sample mean is thus estimated as

$$\text{var}[\overline{s}_n] = \frac{\sigma^2}{n} \approx \frac{1}{2nJ}\sum_{j=1}^{J}[(Z_j^C(n))^2 + (Z_j^S(n))^2]. \tag{12}$$

This estimator is the main result in orthonormally weighted standardized time series (OWSTS) and is called the *J*-th order OWSTS estimator.

In the above construction, Eq (8) is not the only choice for making orthonormality satisfied as in Eq (9). For example, one can construct orthonormal basis under the inner product in the left side of Eq (9) from $\{1,t,t^2,t^3,\cdots\}$ based on the Gram-Schmidt orthogonalization. However, solving for the integral equation with the covariance kernel of Eq (7),

$$\int_0^1 E[B_B(t)B_B(u)]g(t)dt = \lambda g(u), \tag{13}$$

one finds pairs of eigenvalues and eigenfunctions as (Appendix)

$$\lambda_j = 1/(\pi j)^2, \quad e_j(t) = \sqrt{2}\sin(\pi jt), \quad j=1,2,\ldots. \tag{14}$$

The Karuhunen-Loéve expansion of $B_B(t)$ is then formally written down as [21]

$$B_B(t) = \sum_{j=1}^{\infty} \eta_j \sqrt{\lambda_j} e_j(t) = \frac{\sqrt{2}}{\pi} \sum_{j=1}^{\infty} \eta_j \frac{\sin(\pi j t)}{j} \tag{15}$$

where η_j are independent standard normal random variables. The expansion in Eq (15) indicates that weighting functions proportional to $j \times$ (sine or cosine) (π (integer) t) are natural choices. For this reason, the OWSTS estimator with the weighting functions in Eq (10) is used in this work for the statistical error estimation of sample mean.

3. Fractional Brownian Motion and Power Spectrum

Eq (6) asserts that $T_n(t)$ will be under the distribution of $B_B(t)$ for $0 \le t \le 1$ as $n \to \infty$. On the other hand, one cannot exclude the possibility that the real relative error $\sigma / (\mu\sqrt{n})$ is practically small enough when n is not so large as to ensure $T_n(t)$ under the distribution of $B_B(t)$. In this way, one often faces statistical estimation problems under the departure from an ideal distribution and it is natural to introduce an extended model of Brownian motion known as fractional Brownian motion (FBM) [22,23]:

(FBM) (a) $P_R(B_M^F(t+h) - B_M^F(t) \le z) = (2\pi h^{2\alpha})^{-1/2} \int_{-\infty}^{z} \exp(-u^2/(2h^{2\alpha}))du$, $t \ge 0$, $h > 0$, $0 < \alpha < 1$,

(b) $P_R(B_M^F(0) = 0) = 1$ and $B_M^F(t)$ is continuous with probability 1 for $t \ge 0$,

where $B_M^F(t)$ denotes the path of FBM. Hereafter, citation will be made as (FBM), (a) in (FBM), etc. It is clear that (b) and (c) in (BM) is equivalent to (a) and (b) in (FBM) with $\alpha = 0.5$. It follows from (a) and (b) in (FBM) that [18]

$$E[(B_M^F(u+t+h) - B_M^F(u+t))(B_M^F(u+t) - B_M^F(u))]$$

$$= \frac{1}{2}[(t+h)^{2\alpha} - t^{2\alpha} - h^{2\alpha}], u \ge 0, t > 0, h > 0. \tag{16}$$

As the right hand side is zero for $\alpha = 0.5$, (a) in (BM) follows from the equivalence of uncorrelatedness and independence in normal distribution; Brownian motion is FBM with $\alpha = 0.5$. It is also easy to show that the covariance of the adjacent increments of FBM in Eq

(16) is positive or negative, respectively, depending on $0.5<\alpha<1$ or $0<\alpha<0.5$ [22,23]. In addition, by rewriting Eq (16) as

$$\frac{E[(B_M^F(u+t+h)-B_M^F(u+t))(B_M^F(u+t)-B_M^F(u))]}{h^\alpha t^\alpha}=\frac{1}{2}\left[\left(\sqrt{\frac{t}{h}}+\sqrt{\frac{h}{t}}\right)^{2\alpha}-\left(\frac{t}{h}\right)^{\alpha}-\left(\frac{h}{t}\right)^{\alpha}\right], \quad (17)$$

the representative correlation of adjacent increments of FBM is obtained by setting h=t:

$$\mathrm{RC}(\alpha)=2^{2\alpha-1}-1. \quad (18)$$

Note that RC(α) is positive for $0.5<\alpha<1$ and negative for $0<\alpha<0.5$.

In general, tallies in MC criticality calculation are scored by way of paths and collisions of many particles. This can give rise to situations where the fluctuation of $T_n(t)$ in Eq (6) exhibits some characteristics of normal distribution even when the number of generations is not sufficiently large so as to ensure CID in Eqs (5) and (6). Such a scenario indicates the need for the characterization of the departure or deviation from Brownian motion in Eq (5) and Brownian bridge in Eq (6). In advanced stochastic analysis [22], FBM is utilized for the innovation noises under normal distribution containing Brownian motion as a special case of independent increments. In fractal geometry [23], FBM is a stochastic model for continuous and non-differentiable lines with dimensions 1 through 2 and Brownian motion has a dimension of 1.5. These theories indicate that Brownian motion is a case of midway nature in FBM. Moreover, in the path of Brownian bridge $B_B(t)=B_M(t)-tB_M(1)$, the dimension of the first term is 1.5 and that of the second term is 1, which implies that the fluctuation of $B_B(t)$ is strongly dominated by the first term $B_M(t)$. For this reason, spectral comparison will be made for $T_n(t)$ and $B_M(t)$ in Section 4.

Further motivation for the spectral analysis with power spectrum comes from the review of a theoretically less-founded part of the run length diagnosis of MC criticality calculation using fractal dimension analysis [18]. FBM ($B_M^F(t)$) is known to have the dimension of 2-α [23]. It was also shown that the dimension of $B_B(t)$ is equal to that of $B_M(t)$ [18]. Introducing the assumption that the fluctuation of ISTS in MC criticality calculation is

governed by the distribution of $B_M^F(t)$ and thus the path of ISTS has the dimension 2-α, dimension analysis was applied to compute the index α in order to see if 2–α≈1.5 (dimension of $B_M(t)$). The idea is itself sound, however the computational steps involved a linear least square fitting that was merely an ad hoc choice based on numerical observations. We seeks to improve this empiricism.

A frequency representation of FBM was first asserted as [24]

$$B_M^F(t_2) - B_M^F(t_1) \propto \int_0^\infty (e^{2\pi i f t_2} - e^{2\pi i f t_1}) f^{-\alpha-1/2} d\tilde{B}_M(f) \tag{19}$$

where i in the argument of exponentials is the imaginary unit $(i^2 = -1)$, and $\tilde{B}_M(f)$ is the complex Brownian motion process in the frequency domain. Since then, it was widely accepted that Eq (19) implied the $1/f^{2\alpha+1}$ power spectrum of $B_M^F(t)$. However, it was also pointed out that spectral densities of nonstationary random functions such as $B_M^F(t)$ were difficult to interpret [24]. Later, motivated by the stationary property of increments as represented in Eq (16), the power spectrum of a non-stationary stochastic process Y with stationary increments, denoted as $\Phi_Y(\omega)$, was established via the structure function $R_Y(t_2, t_1; t_4, t_3)$ [25]:

$$\begin{aligned} R_Y(t_2, t_1; t_4, t_3) &\equiv E[(Y(t_2) - Y(t_1))(Y(t_4) - Y(t_3))] \\ &= E[Y(t_4)Y(t_2)] - E[Y(t_4)Y(t_1)] - E[Y(t_3)Y(t_2)] + E[Y(t_3)Y(t_1)] \\ &= \frac{1}{2\pi}\int_{-\infty}^{\infty}\left[e^{i\omega(t_4-t_2)} - e^{i\omega(t_4-t_1)} - e^{i\omega(t_3-t_2)} + e^{i\omega(t_3-t_1)}\right]\Phi_Y(\omega)d\omega\,. \end{aligned} \tag{20}$$

In this framework, the power spectrum of FBM was derived to be [25]

$$\Phi_{B_M^F}(\omega) = \frac{1}{|\omega|^{2\alpha+1}}\quad. \tag{21}$$

Now, given a realization $\hat{Y}(t)$ of the real-valued stochastic process $Y(t)$ with mean zero and stationary increments, the power spectrum is defined in an asymptotically computable manner [23]:

$$\hat{\Phi}_Y(\omega) \equiv \lim_{P\to\infty} \frac{1}{2P}\left|\int_{-P}^{P} \hat{Y}(t)e^{i\omega t}dt\right|^2 \quad (22).$$

(Note that $\hat{Y}$ is assumed to be real and a squared-absolute value is computed for integral.) Similarly, the covariance of $Y(t)$ is also defined in an asymptotically computable manner:

$$\hat{C}(h) \equiv \lim_{P\to\infty} \frac{1}{2P}\int_{-P}^{P} \hat{Y}(t)\hat{Y}(t+h)dt\,. \quad (23)$$

The power spectrum in Eq (22) is shown to be the Fourier transform of the covariance in Eq (23) as asserted in the Wiener-Khinchin theorem [23]:

$$\hat{\Phi}_Y(\omega) = \int_{-\infty}^{\infty} \hat{C}(h)e^{-i\omega h}dh\,. \quad (24)$$

The inverse Fourier transform of Eq (24) reads

$$\hat{C}(h) = \frac{1}{2\pi}\int_{-\infty}^{\infty} e^{i\omega h}\hat{\Phi}_Y(\omega)d\omega\,. \quad (25)$$

Eqs (23) and (25) correspond to term-wise equality in Eq (20); equating $\hat{\Phi}_Y(\omega)$ and $\hat{C}(h)$, respectively, to $\Phi_Y(\omega)$ and $E[Y(t)Y(t+h)]$ do not introduce any inconsistency in Eq (20). Therefore, Eq (21) also implies the following relation for $\hat{B}_M^F(t)$:

$$\hat{\Phi}_{B_M^F}(\omega) = \lim_{P\to\infty} \frac{1}{2P}\left|\int_{-P}^{P} \hat{B}_M^F(t)e^{-i\omega t}dt\right|^2 = \frac{1}{|\omega|^{2\alpha+1}}\,, \quad (26)$$

where the hat in $\hat{B}_M^F(t)$ implies a realization as in $\hat{Y}(t)$. If one views $T_n(t)$ as a periodic function with a period of 1, the power spectrum of ISTS is expressed as

$$\Phi_{T_n}(\omega) = \left|\int_0^1 T_n(t)e^{-i\omega t}dt\right|^2 \quad (27)$$

Using the frequency f instead of the angular frequency ω, Eq (27) can be computed as

$$\Phi_{T_n}(f) = \left|\frac{1}{n}\sum_{j=1}^{n-1} T_n\left(\frac{j}{n}\right)e^{-i2\pi f\frac{j}{n}}\right|^2\,. \quad (28)$$

Here j=0 and n are excluded from the summation because $T_n(0)$=$T_n(1)$=0.

For reference purposes, it will be instructive to compute $\Phi_{B_M^F}(f)$ from a realization of $B_M^F(t)$. To this end, based on the following relation similar to Eq (16) [23]

$$E[B_M^F(t)B_M^F(t+h)] = \frac{1}{2}[t^{2\alpha} + (t+h)^{2\alpha} - h^{2\alpha}], \tag{29}$$

the covariance matrix $\mathbf{C} = (C_{j,k})$ of $B_M^F(t)$ is introduced as

$$C_{j,k} \equiv E[B_M^F(t_j)B_M^F(t_k)] = \frac{1}{2}[t_j^{2\alpha} + t_k^{2\alpha} - |t_j - t_k|^{2\alpha}], \;\; t_j = \frac{j}{n}, t_k = \frac{k}{n}, \;\; j,k = 1,\ldots,n. \tag{30}$$

Since covariance matrices are symmetric and non-negative definite, Cholesky factorization allows one to express the matrix **C** as the product of a lower triangular matrix **L** and its transpose $\mathbf{L}^{\mathrm{T}}$:

$$\mathbf{C} = (C_{i,j}) = \mathbf{L}\mathbf{L}^{\mathrm{T}}. \tag{31}$$

Let $\mathbf{V} \equiv (V_1, V_2, \ldots, V_n)$ be a vector of independent random variables under the standard normal distribution satisfying $E[V_j]=0$, $E[(V_j)^2]=1$ and $E[V_jV_k]=0$ for $j \neq k$ where the subscripts of V_j and V_k corresponds to t_j and t_k. The covariance matrix of **LV** then becomes equal to $\mathbf{C} = \mathbf{L}\mathbf{L}^{\mathrm{T}}$. Therefore, sampling $(V_1, V_2, \ldots, V_n)$, one obtains a realization of B_M^F as

$$\left(\hat{B}_M^F(t_1), \hat{B}_M^F(t_2), \ldots, \hat{B}_M^F(t_n)\right) = (\mathbf{L}\mathbf{V})^T. \tag{32}$$

For this realization of $B_M^F(t)$, one can compute

$$\Phi_{B_M^F}(f) \approx \left| \frac{1}{n} \sum_{j=1}^{n} \hat{B}_M^F\left(\frac{j}{n}\right) e^{-i2\pi f \frac{j}{n}} \right|^2 \propto \frac{1}{f^{2\alpha+1}}. \tag{33}$$

Here, the proportionality to $1/f^{2\alpha+1}$ is displayed due to Eq (26). For Brownian motion, $\alpha = 0.5$ yields

$$\Phi_{B_M}(f) \approx \left| \frac{1}{n} \sum_{j=1}^{n} \hat{B}_M\left(\frac{j}{n}\right) e^{-i2\pi f \frac{j}{n}} \right|^2 \propto \frac{1}{f^2} \tag{34}$$

On the other hand, the Fourier transform of $t\hat{B}_M(1)$ is

$$\int_0^1 t\hat{B}_M(1) e^{-2\pi i f t} dt = \hat{B}_M(1)\left[\frac{e^{-2\pi i f}}{(-2\pi i f)} - \frac{e^{-2\pi i f} - 1}{(-2\pi i f)^2} \right] \approx \frac{\hat{B}_M(1)e^{-2\pi i f}}{(-2\pi i f)} \quad \text{for} \quad f \gg 1. \tag{35}$$

This implies that $tB_M(1)$ does not introduce a frequency component attenuating slower than $1/f^2$ in the power spectrum of $B_B(t)$. Therefore, Eqs (34) and (35) yield

$$\Phi_{B_B}(f) \approx \left| \frac{1}{n} \sum_{j=1}^{n} \left[\hat{B}_M\left(\frac{j}{n}\right) - \frac{j}{n} \hat{B}_M(1) \right] e^{-i2\pi f \frac{j}{n}} \right|^2 \propto \frac{1}{f^2} \quad \text{for} \quad f \gg 1, \tag{36}$$

i.e., the power spectrum of Brownian bridge is also proportional to $1/f^2$ except for small frequencies. It then follows from Eq (6) that

$$\Phi_{T_n}(f) = \left| \frac{1}{n} \sum_{j=1}^{n-1} T_n\left(\frac{j}{n}\right) e^{-i2\pi f \frac{j}{n}} \right|^2 \propto \frac{1}{f^2} \quad \text{for} \quad f \gg 1 \quad \text{as} \quad n \to \infty \ . \tag{37}$$

At this stage of developments, it is worthwhile repeating the issue raised at the beginning of this section: A scenario cannot be excluded that the real relative error $\sigma/(\mu\sqrt{n})$ is practically small enough when *n* is not so large as to ensure $T_n(t)$ under the distribution of $B_B(t)$. To cope with this non-ideal issue of practical interest, one may place the following hypothesis on numerical testing:

$$\left(\begin{matrix} n \text{ is sufficiently large but not} \\ \text{so large as to ensure CID} \end{matrix} \right) \Rightarrow \Phi_{T_n}(f) \propto \frac{1}{f^{2\alpha+1}}, \alpha \neq 0.5 \quad \text{for} \quad f \gg 1. \tag{38}$$

Here, "*n* is sufficiently large" is captured by the normality attribute of FBM while "but not so large as to ensure CID" is reflected in $\alpha \neq 0.5$.

In the CID of $T_n(t)$ toward $B_B(t) = B_M(t) - tB_M(1)$, fractal dimension is 1.5 and 1.0, respectively, for the first and second terms of $B_B(t)$ [18,23]. The fluctuation of $B_B(t)$ is thus dominated by the first term ($B_M(t)$) and the insufficient CID of $T_n(t)$ will appear as the FBM characteristics with $\alpha \neq 0.5$. Consequently, $T_n(t)$ in Eq (6) and $\lfloor nt \rfloor (s_{\lfloor nt \rfloor} - \mu)/(\sigma\sqrt{n})$ in Eq (5) are both likely to exhibit the normality characteristics of FBM with $\alpha \neq 0.5$ when *n* is sufficiently large but not so large as to ensure CID. Taking into account that the standard normality of $B_M^F(1)$ follows from setting $t = 0$ and $h = 1$ in (FBM) and $\lfloor nt \rfloor (s_{\lfloor nt \rfloor} - \mu)/(\sigma\sqrt{n})$ in Eq (5) becomes $(s_n - \mu)/(\sigma/\sqrt{n})$ for $t = 1$, one can form the confidence interval of s_n based on normality assumption and the inverse square-root

law of decrease will be observed for the standard deviation of s_n if the accurate estimate of σ is available. These matters can be judged based on Eq (38).

Before concluding this section, it is worth raising the second reason for choosing the weighting functions in Eq (8) in addition to the first reason mentioned at the end of Section 2. In this section, the power spectrum of $B_B(t)$ was shown to be proportional to $1/f^2$. The functions $\sin(2\pi jt)$ and $\cos(2\pi jt)$ correspond to the components of integer frequency j. Under these characteristics, the weighting functions should be proportional to (inverse square root of power spectrum at frequency j) × (sine or cosine) $(2\pi jt)$ so that equal contributions are extracted from all integer frequencies. This argument gives another legitimacy to a choice in Eq (8).

4. Local Power Tally in PWR Whole Core Calculation – Numerical Results 1

In this section, numerical results are demonstrated for power spectrum, the α-index in (a) in (FBM) that subsequently appeared in Eqs (33) and (38), and the standard deviation estimation by OWSTS in Eq (12) for a model of PWR initial core in **Figure 1**. Since the previous investigation of this model [9] has revealed that the autocorrelation of local power tallies is generally largest at the fifth assembly along diagonal from center, the local power at the location indicated in Fig. 1 is examined in this section. The effective neutron multiplication factor (k_{eff}) is also examined for comparison. Power spectrum is computed for the frequencies $10^{0.05*j}$, $j = 20,\ldots,60$, so that $10 \le f \le 1000$ is covered. All MC calculations are conducted by a version of the MCNP code with ENDF-VI libraries [26] The detailed specifications of the model in Fig. 1 are available in previous work [15].

Figure 2 shows the reference power spectrum from a replica of Brownian motion computed by Eq (34) and the power spectra of ISTS ($T_n(t)$) for the k_{eff} and local power of PWR in Fig. 1 computed by Eq (28). It is seen that the power spectrum of k_{eff} nearly follows the $1/f^2$ law as does the power spectrum of Brownian motion. **Figure 3** shows the α-index values obtained from the power spectra of 100 independent replicas of Brownian motion. It

follows that RC(α) in Eq (18) falls within –0.09 and 0.09 for the uncertainty of the one-replica standard deviation of α. The fluctuations in Fig.3 indicate that in Fig. 2 the deviation from the α-index value at CID, i.e., the deviation from 0.5, is within statistical uncertainty for k_{eff} but well beyond statistical uncertainty for the local power; RC(α)=–0.03 and 0.66, respectively, for the k_{eff} and local power. However, the power spectrum of local power still exhibits the $1/f^{2\alpha+1}$ law of FBM. This was observed for other replicas of the MC calculation with the same computational conditions (n=4500, and 100000 particles per generation), which are not shown here to avoid repetitions of similar figures. Namely, the hypothesis in Eq (38) has been confirmed for the model in Fig. 1 and it is thus possible to assume normality on the sample mean s_n. The remaining issues are to check whether or not the α-index estimates converge rapidly toward 0.5 as n increases and to see if it is possible to make the unbiased estimation of the standard deviation of sample mean ($\sigma/\sqrt{n}$) before CID is achieved. **Figure 4** shows the α index of local power for 10 independent replicas of MC calculation. It is obvious that CID will not occur for $n \le 18000$ for the computation with 100000 particles per generation; the convergence in terms of CID is very slow for local power tally. Two specific issues can be raised from this result; is it possible to make unbiased estimation of the standard deviation of the sample mean s_n for $n \le 18000$ and does the power spectrum of $T_n(t)$ keep the spectral form of the $1/f^{2\alpha+1}$ law of FBM for the replica i yielding rapidly changing estimates of α-index? Both issues are answered positively as shown in **Figures 5** and **6**. Fig 5 shows that the standard deviation of s_n can be estimated in an unbiased manner by OWSTS if the real statistical error is about 1% or smaller corresponding to $n \ge 9000$. Fig 6 demonstrates that the rapidly changing power spectra at n=6000, 9000 and 12000 for replica i in Fig. 4 maintain the spectral form of FBM, which is a further confirmation of the hypothesis in Eq (38). These numerical results indicate that even before CID is achieved, the standard deviation of sample mean can be estimated in an unbiased manner and a confidence interval may be formed based on normality assumption if the real

statistical error is sufficiently small. Figs 4 and 5 confirm the appearance of the pre-CID phenomenon mentioned in Sec 1. It is also worth mentioning that, associated with the jump-up and jump-down of the α-index estimates from 0.69 via 0.95 to 0.64 for replica *i* in Figs 4 and 6, RC(α) in Eq (18) changes from 0.31 via 0.87 to 0.21 while the spectral form in Fig 6 maintains the $1/f^{2\alpha+1}$ law of FBM. Wild changes may occur in the α-index estimates while keeping the spectral form of FBM. This phenomenon is a new discovery as far as this author is aware of. Moreover, in Fig 6 and in the third figure of Fig 2, the spectral form of FBM leans toward the side of $1/f^2$ through $1/f^3$ ($0.5<\alpha<1$). This implies that the higher frequency components of $T_n(t)$ are smaller in magnitude than they are supposed to be. Consequently, improvement in the OWSTS estimator is not likely to occur by further raising the order *J* because of the correspondence between integer frequencies and the orders of OWSTS weighting functions discussed at the end of Section 3. For this reason, *J* is fixed to 10 in Fig 5 as practiced in previous work [12].

5. Effective Neutron Multiplication Factor (k_{eff}) in Fuel Debris Model - Numerical Results 2

In this section, numerical results are demonstrated for a preliminary model of UO_2-concrete debris in **Figure 7** [16]. The model geometry is a cube of 140×140×140 cm^3; inside this cube, a smaller inner cube of 100×100×100 cm^3 is situated at center with the corresponding faces parallel to each other; the inner cube is occupied by concrete and UO_2 fuel at 12 GWd/t with the average volume ratio of 7:1 in concrete:UO_2; the outside of the inner cube is occupied by concrete only. One energy group macroscopic cross-sections in Fig. 7 were computed by the MVP code [1]. MC criticality calculations are carried out with an in-house research-purpose code.

Concerning the mixture of concrete and UO_2 fuel inside the inner cube, the macroscopic cross-section of reaction-type *RT* is assigned by

$$\Sigma_{RT}(\mathbf{r}) = \nu(1+\Delta\nu(\mathbf{r}))\Sigma_{RT}^{F} + [1-\nu(1+\Delta\nu(\mathbf{r}))]\Sigma_{RT}^{C} \tag{39}$$

where unlike Sections 2 and 3, the italic Σ is not the summation symbol but the Greek letter "sigma" as traditionally used for macroscopic cross-section in nuclear reactor physics, $\mathbf{r} = (x_1, x_2, x_3)$ is the space coordinates inside the inner cube in Fig. 7, the superscripts *F* and *C* indicate, respectively, the UO_2 fuel and concrete, v=1/8 is the mean volume fraction of fuel, and $\Delta v(\mathbf{r})$ is the space-dependent variation part of the volume fraction of fuel. The randomized Weierstrass function (RWF) [16] is assigned to $\Delta v(\mathbf{r})$:

$$\Delta v(\mathbf{r}) = d\sum_{j=1}^{\infty} B_j \lambda^{-\alpha j} \sin(\lambda^j (\mathbf{r}/R) \bullet \mathbf{\Omega}_j + A_j), \tag{40}$$

where the non-italic Σ is the summation symbol as in Sections 2 and 3, d is the parameter determining the level of fluctuation, B_j are the independent Bernoulli random variables taking ±1 equally likely, λ>1, R is the scaling factor, $\mathbf{\Omega}_j$ are unit vectors chosen uniformly and independently on the unit sphere at the origin, and A_j are independent random variables uniformly distributed on [0,2π). As B_j, $\mathbf{\Omega}_j$ and A_j are independent and the expected value of B_j is zero, the expected value of $\Delta v(\mathbf{r})$ is zero. The parameter α in Eq (40) satisfies $0 < \alpha \le 0.5$ so that $\Delta v(\mathbf{r})$ represents a stationary approximation [16] to the system state reached via extreme disorder [27] characterized by the power spectrum of $1/f^{1+2\alpha}$. For this reason, the same parameter α is used in Eqs (33), (38) and (40). Practically, when the summation in Eq (40) is truncated at $j=M$, d is chosen to be

$$d = \frac{\lambda^{\alpha} - 1}{1 - \lambda^{-\alpha M}} \tag{41}$$

so that $-1 \le \Delta v(\mathbf{r}) \le 1$ is satisfied [16]. The number of terms M for the summation truncation is chosen to be the smallest positive integer satisfying $\lambda^{-\alpha M} < 0.01$. In other words, the terms in Eq (40) are kept as far as their amplitudes are larger than 1% of the amplitude of the first term.

Figure 8 shows OWSTS estimates together with apparent estimates for the standard deviation of the sample mean of k_{eff} tallies; a pair of these estimates are shown for each of 100

independent replicas of RWF. It is clearly seen that OWSTS estimates are on average significantly larger than apparent estimates and under large fluctuation. It is desirable to clarify if these fluctuation is a spurious phenomenon due to insufficient CID. To this end, power spectra are shown in **Figure 9** for the replicas yielding the largest and smallest OWSTS estimates in Fig. 8. If judged based on the fluctuation in Fig 3, it is clear that both power spectra exhibit the $1/f^{2\alpha+1}$ law with $\alpha = 0.5$. Power spectra for other replicas of RWF were also examined and turned out to follow the $1/f^{2\alpha+1}$ law with $\alpha = 0.5$, which is not included here to avoid the repetitions of similar figures. It is deemed certain that estimates in Fig.8 are obtained under CID and their fluctuation is not spurious and is attributed to the different correlation properties of k_{eff} tallies due to randomly realized replicas of RWF. **Figure 10** shows OWSTS estimates of the standard deviation of sample mean with respect to the order *J* in Eq (12) for additional 10 replicas after replica 100 in Fig 8. There is no sign of ill behaviors such as divergence, zeroing-out, rapid swing at very large orders which may arise from insufficient CID.

6. Conclusions

In this work, the spectral analysis of the interpolated standardized time series (ISTS) of tallies was proposed to assess convergence in distribution (CID) in the framework of the central limit theorem. It was shown that via the Fourier transform of ISTS one could compute power spectrum which was to be compared with the inverse-square dependence on frequencies because of CID toward Brownian bridge. The criterion is universal, which is the strength of the proposed methodology. Modeling with fractional Brownian motion was also attempted at in order to capture the departure from the ideal state of CID. These methodologies were demonstrated for models of PWR initial core [15] and UO_2-concrete debris [16].

Salient aspects of numerical results are summarized as below. First, in the model of PWR initial core, the power spectrum from local power tallies was under the law expected for

fractional Brownian motion. This means that even before CID is achieved, one is allowed to form a confidence interval based on normality assumption if the standard deviation of sample mean can be estimated in an unbiased manner. Specifically, the unbiased estimation of the standard deviation of sample mean during insufficient CID generations leads to the pre-CID phenomenon raised in Sec 1, which was indeed observed when real relative statistical errors were about 1% or smaller. Second, in the model of UO_2-concrete debris, CID is achieved for the tallies of effective neutron multiplication factor and the standard deviation estimation of sample mean with orthonormally weighted standardized time series (OWSTS) performed normally without any indication of ill behaviors such as divergence, zeroing-out and rapid swing at very large orders. Based on this result, the following guideline may be placed on the standard deviation estimation with OWSTS; do not raise the order beyond 10 as recommended in previous work [12] unless CID is judged to be achieved by the power spectrum of ISTS.

In future work, technical tools in stochastic differential equations may be pursued so that ISTS is transformed to other statistic which is asymptotically under the law of Brownian motion. One can then develop improved statistical methodologies based on 1) the independent increments of Brownian motion for non-overlapping intervals and 2) the inference procedures for the stochastic processes driven by Brownian motion. In pursuit of these developments, estimation instability inherent in cases of a small number of generations should be appropriately addressed.

Acknowledgments

Work reported in this paper was performed under the auspices of the Nuclear Regulation Authority (NRA) / the Secretariat of NRA of Japan.

The author is thankful to Dr. K Tonoike, Nuclear Safety Research Center, Japan Atomic Energy Agency, for the support of Monte Carlo methodology development.

Appendix: Eigenfunctions and Eigenvalues of Eq (13)

This appendix shows how to obtain the eigenvalues and eigenfunctions of Eq (13),

$$\int_0^1 [\min(t,u) - tu] g(t) dt = \lambda g(u), \tag{42}$$

where Eq (7) is substituted in Eq (13). First, rewrite Eq (42) as

$$\int_0^u tg(t)dt + u\int_u^1 g(t)dt - u\int_0^1 tg(t)dt = \lambda g(u). \tag{43}$$

Differentiate with respect to u:

$$\int_u^1 g(t)dt - \int_0^1 tg(t)dt = \lambda g'(u). \tag{44}$$

Differentiate once more to yield

$$g''(u) = -\frac{1}{\lambda} g(u). \tag{45}$$

The general solution of Eq (42) is then obtained as

$$g(u) = A\sin\left(\frac{u}{\sqrt{\lambda}}\right) + B\cos\left(\frac{u}{\sqrt{\lambda}}\right) \quad . \tag{46}$$

Since Eq (42) implies $g(0) = 0$, one obtains $B = 0$. Eq (42) also implies $g(1) = 0$, which leads to $\lambda = 1/(\pi j)^2$, $j = 1, 2, \ldots$:

$$g(u) = A\sin(\pi j u), \quad j = 1, 2, \ldots. \tag{47}$$

Finally, the normalization condition $\int_0^1 [g(u)]^2 du = 1$ yields $A = \sqrt{2}$.

References

[1] Nagaya Y, Okumura K, Mori T, Nakagawa M. MVP/GMVP II: General Purpose Monte Carlo Codes for Neutron and Photon Transport Calculations Based on Continuous Energy and Multigroup Methods. Tokai-mura, Ibaraki-ken (Japan): Japan Atomic

Energy Agency; 2005, JAERI-1348

[2] Goorley JT. MCNP6.1.1-Beta Release Notes. Los Alamos, NM (USA): Los Alamos National Laboratory; 2014, LA-UR-14-24680.

[3] Brun E, Damian F, Diop CM, Dumonteil E, Hugot FX, Jouanne C, Lee YK, Malvagi F, Mazzolo A, Petit O, Trama JC, Visonneau T, Zoia A. TRIPOLI-4®, CEA, EDF and AREBA Reference Monte Carlo Code. Annals of Nuclear Energy. 2015; 82, 151-160.

[4] Lux I, Koblinger L Monte Carlo Particle Transport Methods: Neutron and Photon Calculations. Boca Raton, FL (USA): CRC Press; 1991.

[5] Gelbard EM, Prael R. Computation of Standard Deviations in Eigenvalue Calculations. Progress in Nuclear Energy. 1990; 24, 237-241.

[6] Ueki T, Mori T, Nakagawa M. Error Estimations and Their Biases in Monte Carlo Eigenvalue Calculations. Nuclear Science and Engineering. 1997; 125, 1-11.

[7] Demaret L, Nouli A, Carraro L, Jacquet O. Accurate Determination of Confidence Intervals in Monte Carlo Eigenvalue Calculations. Proc. ICNC'99, Sixth International Conference on Nuclear Criticality Safety; 1999 Sep 20-24; Versailles (France). Vol. 1, 66-80.

[8] Ueki T. Standard Deviation of Local Tallies in Global Monte Carlo Calculation of Nuclear Reactor Core. Journal of Nuclear Science and Technology. 2010; 47, 8, 739-753.

[9] Ueki T. Robust Statistical Error Estimation of Local Power Tallies in Monte Carlo Calculation of Light Water Reactor. Nuclear Science and Engineering. 2015; 180, 58–68.

[10] Park HJ, Lee HC, Shim HJ, Cho JY. Real Variance Analysis of Monte Carlo Eigenvalue Calculation by McCARD for Beavrs Benchmark. Annals of Nuclear Energy. 2016; 90, 205-211.

[11] Griesheimer PD, Nease BR. Spectral Analysis of Stochastic Noise in Fission Source

Distributions from Monte Carlo Eigenvalue calculations. Progress in Nuclear Science and Technology. 2011; 2, 706-715.

[12] Ueki T. An Orthonormally Weighted Standardized Time Series for the Error estimation of Local Tallies in Monte Carlo Criticality Calculation. Nuclear Science and Engineering. 2012; 171, 220-230.

[13] Schruben L. Confidence Interval Estimation Using Standardized Time Series. Operations Research. 1983; 31, 6,1090-1108.

[14] Foley RD, Goldsman D. Confidence Intervals Using Orthonormally Weighted Standardized Time Series. ACM Transactions on Modeling and Computer Simulation. 1999; 9, 4, 297-325.

[15] Nakagawa M, Mori T. Whole Core Calculations of Power Reactors by Use of Monte Carlo Method. Journal of Nuclear Science and Technology. 1993; 30, 7, 692-701.

[16] Ueki T. Monte Carlo Criticality Analysis Under Material Distribution Uncertainty. Journal of Nuclear Science and Technology. 2017; 54, 3, 267-279.

[17] Brockwell PJ, Davis RA. Time Series: Theory and Models, 2nd Ed. New York, NY (USA): Springer; 1991.

[18] Ueki T. Fractal Dimension Analysis for Run Length Diagnosis of Monte Carlo Criticality Calculation. Journal of Nuclear Science and Technology. 2016; 53, 3, 312-322.

[19] Durrett R. Probability: Theory and Examples, 2nd Ed. Belmont CA (USA): Wadsworth Publishing Company; 1996.

[20] Billingsley P. The Lindeberg-Lévy Theorem for Martingales. Proceedings of the American Mathematical Society. 1961; 12, 5, 788-792.

[21] Ghanem RG, Spanos PD. Stochastic Finite Elements: A Spectral Approach. New York NY (USA): Springer-Verlag; 1991.

[22] Biagini F, Hu Y, Øksendal B, Zhang T. Stochastic Calculus for Fractional Brownian

Motion and Applications. London (UK): Springer; 2008.

[23] Falconer K. Fractal Geometry: Mathematical Foundations and Applications, 2nd Ed. West Sussex (England): John Wiley & Sons Ltd; 2003.

[24] Mandelbrot BB, Van Ness JW. Fractional Brownian Motion, Fractional Noises and Applications. SIAM Review. 1968; 10, 4, 422-437. Reprint in Mandelbrot BB. Gaussian Self-Affinity and Fractals. New York NY (USA): Springer-Verlag; 2002.

[25] Reed IS, Lee PC, Truong TK. Spectral Representation of Fractional Brownian Motion in n Dimensions and its Properties. IEEE Transactions on Information Theory. 1995; 41, 5, 1439-1451.

[26] X-5 Monte Carlo Team. MCNP – A General Purpose Monte Carlo N-Particle Transport Code, Version 5. Los Alamos, NM (USA): Los Alamos National Laboratory; 2003, LA-UR-03-1987.

[27] Frieden B.R. Spectral 1/f Noise Derived from Extremized Physical Information. Physical Review E 1994; 49(4): 2644-2649.

Figure Captions

Figure 1. PWR initial core model; local power evaluated for selected cell location at 5th assembly on diagonal in 5th elevation; computations with point-wise cross sections conducted under 100,000 histories per generation for the whole core of this model.

Figure 2. Power spectrum (PS) of Brownian motion compared against PS of interpolated standardized time series from PWR initial core model; results for one replica

Figure 3. a-index estimates of Brownian motion on [0,1] via power spectrum over 100 replicas of paths.

Figure 4. a-index estimates via power spectrum of interpolated standardized time series of local power tally.

Figure 5. Standard deviation (SD) estimation of sample mean (s_n: Eq (4)) of local power tallies by orthonormally weighted standardized time series (OWSTS: J=10) over 60 replicas of a MC computation of 100,000 particles per generation.

Figure 6. Power spectrum (PS) of replica i in Figure 4.

Figure 7. UO_2-Concrete debris model.

Figure 8. Standard deviation estimates of effective neutron multiplication factor (k_{eff}) of UO_2-concrete debris model; one whole set of MC criticality calculation consisting of 20000 particles per generation, 5000 generations and 1000 skip generations for each of 100

independent replicas of randomized Weierstrass function (RWF: a=0.5, l=0.5, *R*=25cm); OWSTS for orthonormally weighted standardized time series estimates.

Figure 9. Power spectrum (PS) of interpolated standardized time series of effective neutron multiplication factor (k_{eff}) in UO_2-concrete debris model with randomized Weierstrass function (RWF).

Figure 10. Converging behaviors of OWSTS standard deviation estimates of effective neutron multiplication factor of UO_2-concrete debris model; 10 independent realizations of randomized Weierstrass function (RWF: a=0.25, l=1.5, *R*=25) replicas; OWSTS for orthonormally weighted standardized time series estimates.

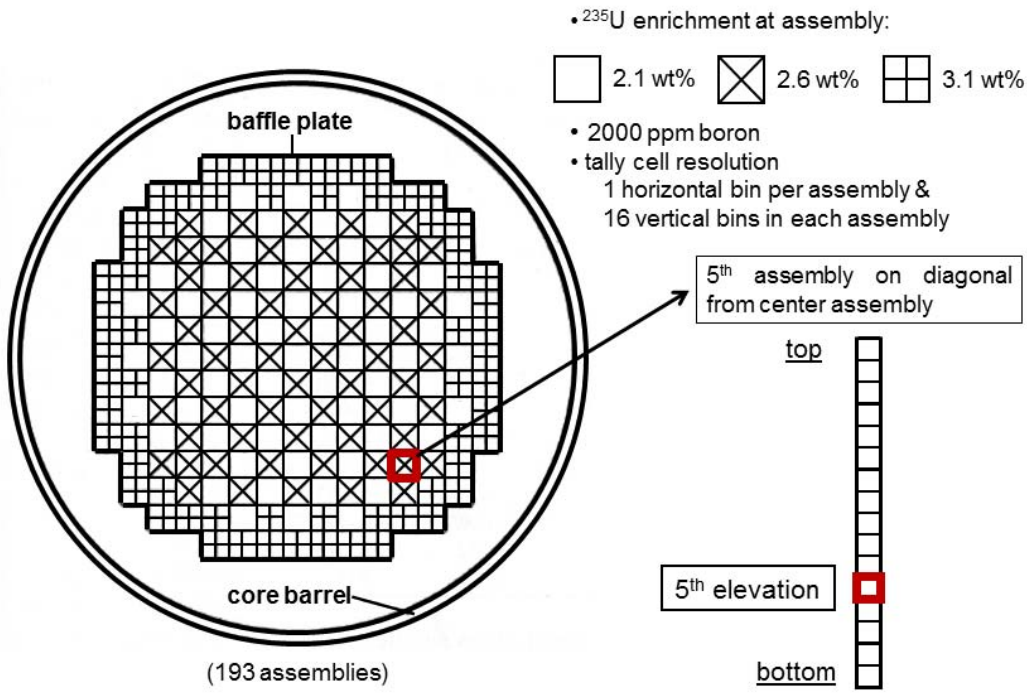

Figure 1. PWR initial core model; local power evaluated for selected cell location at 5th assembly on diagonal in 5th elevation; computations with point-wise cross sections conducted under 100,000 histories per generation for the whole core of this model.

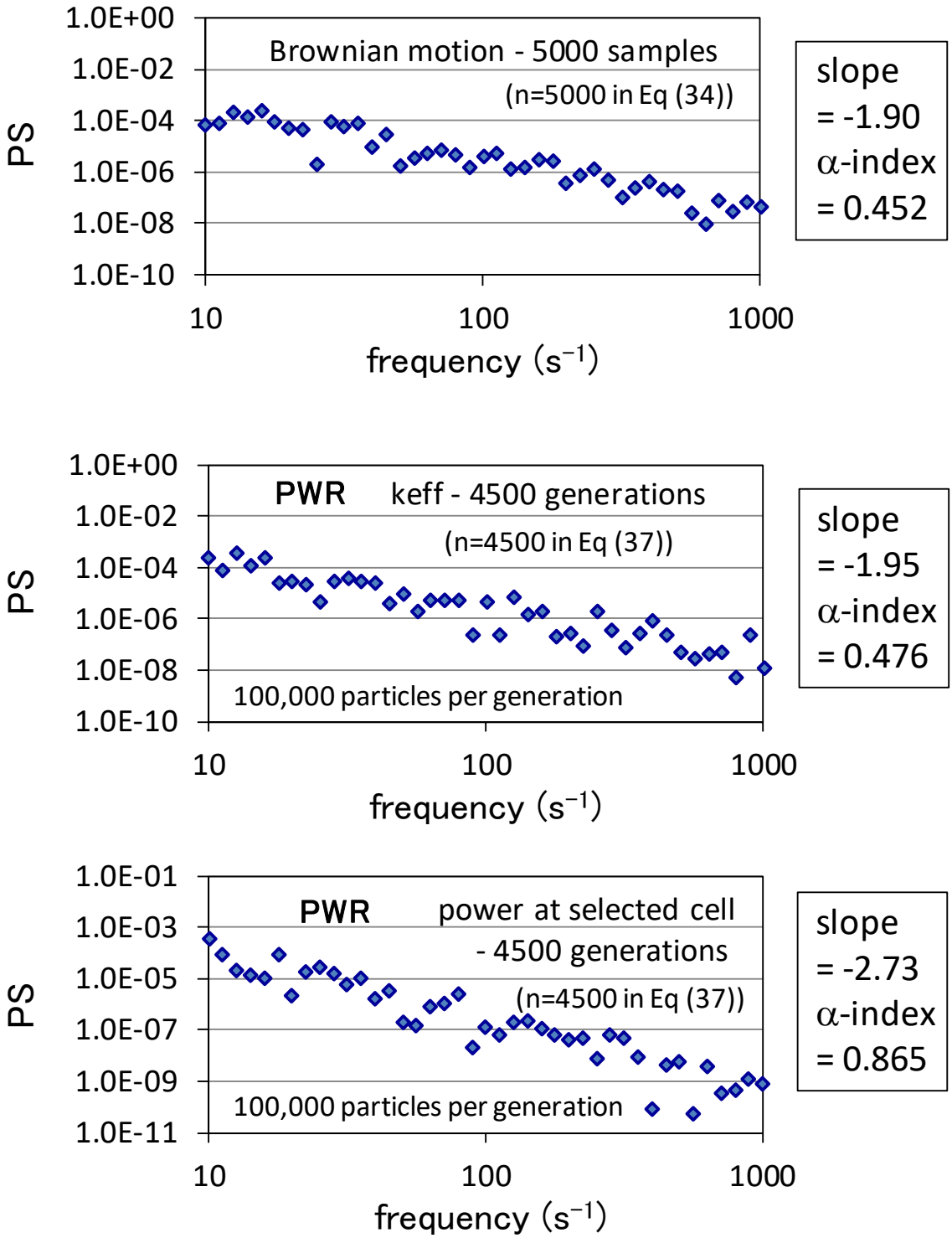

Figure 2. Power spectrum (PS) of Brownian motion compared against PS of interpolated standardized time series from PWR initial core model; results from one replica

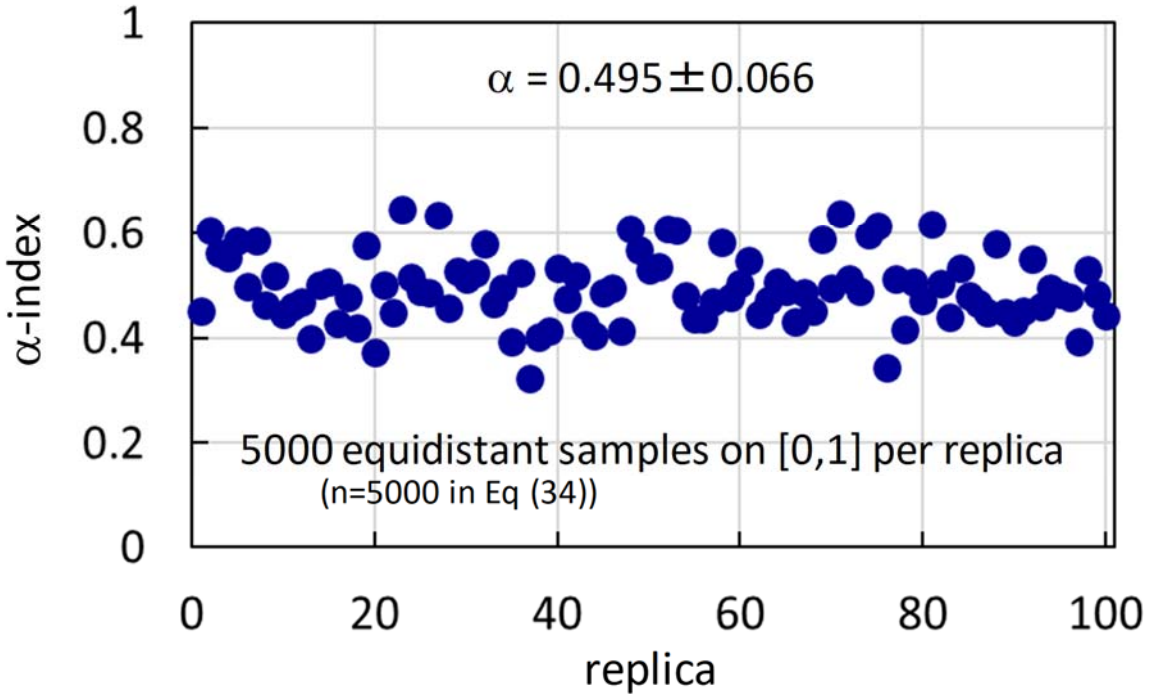

Figure 3. α-index estimates of Brownian motion on [0,1] via power spectrum over 100 replicas of paths.

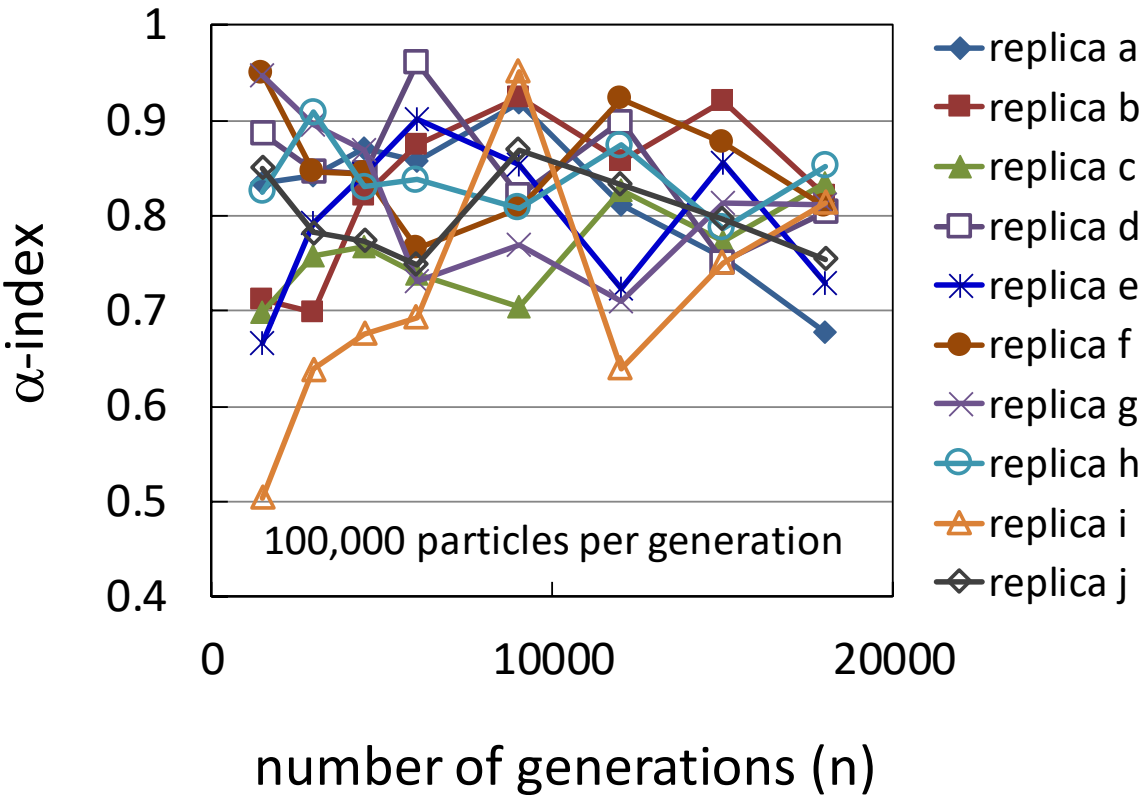

Figure 4. α-index estimates via power spectrum of interpolated standardized time series of local power tallies.

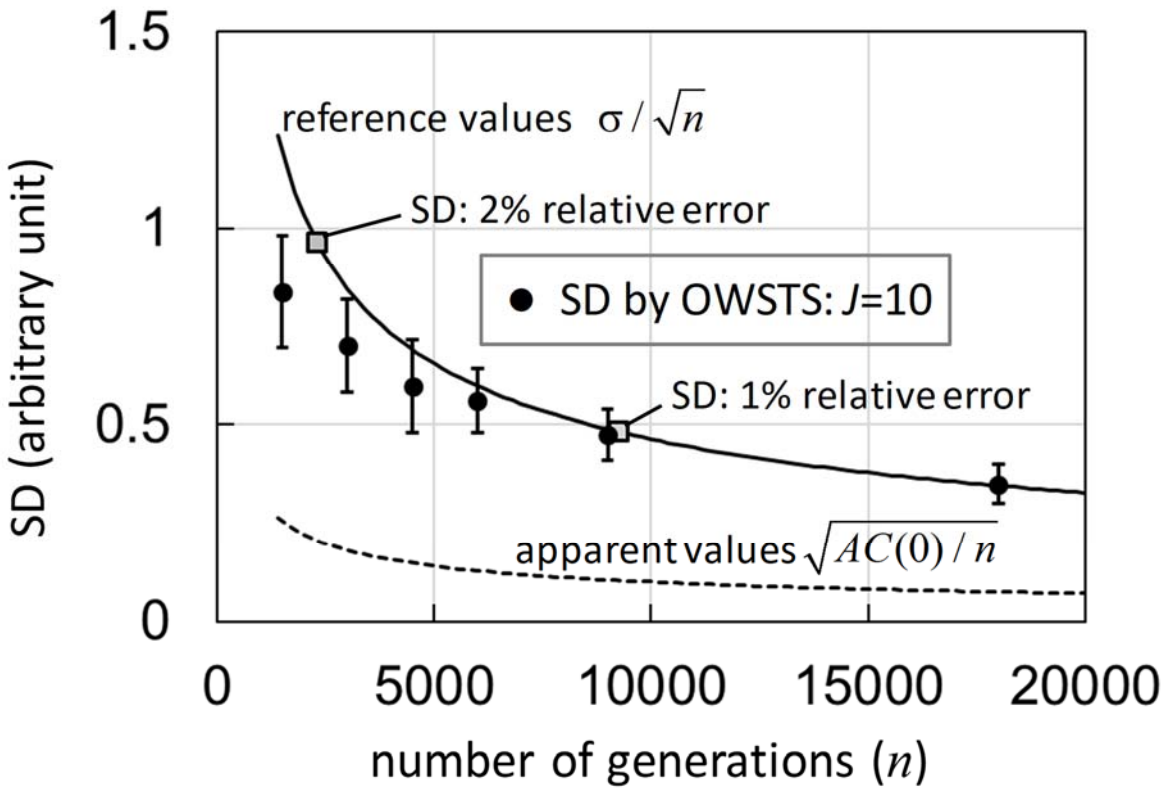

Figure 5. Standard deviation (SD) estimation of sample mean (s_n: Eq (4)) of local power tallies by orthonormally weighted standardized time series (OWSTS: J=10) over 60 replicas of a computation of 100,000 particles per generation; error bars for one replica estimate, i.e., for a population of 60 SD estimates by OWSTS.

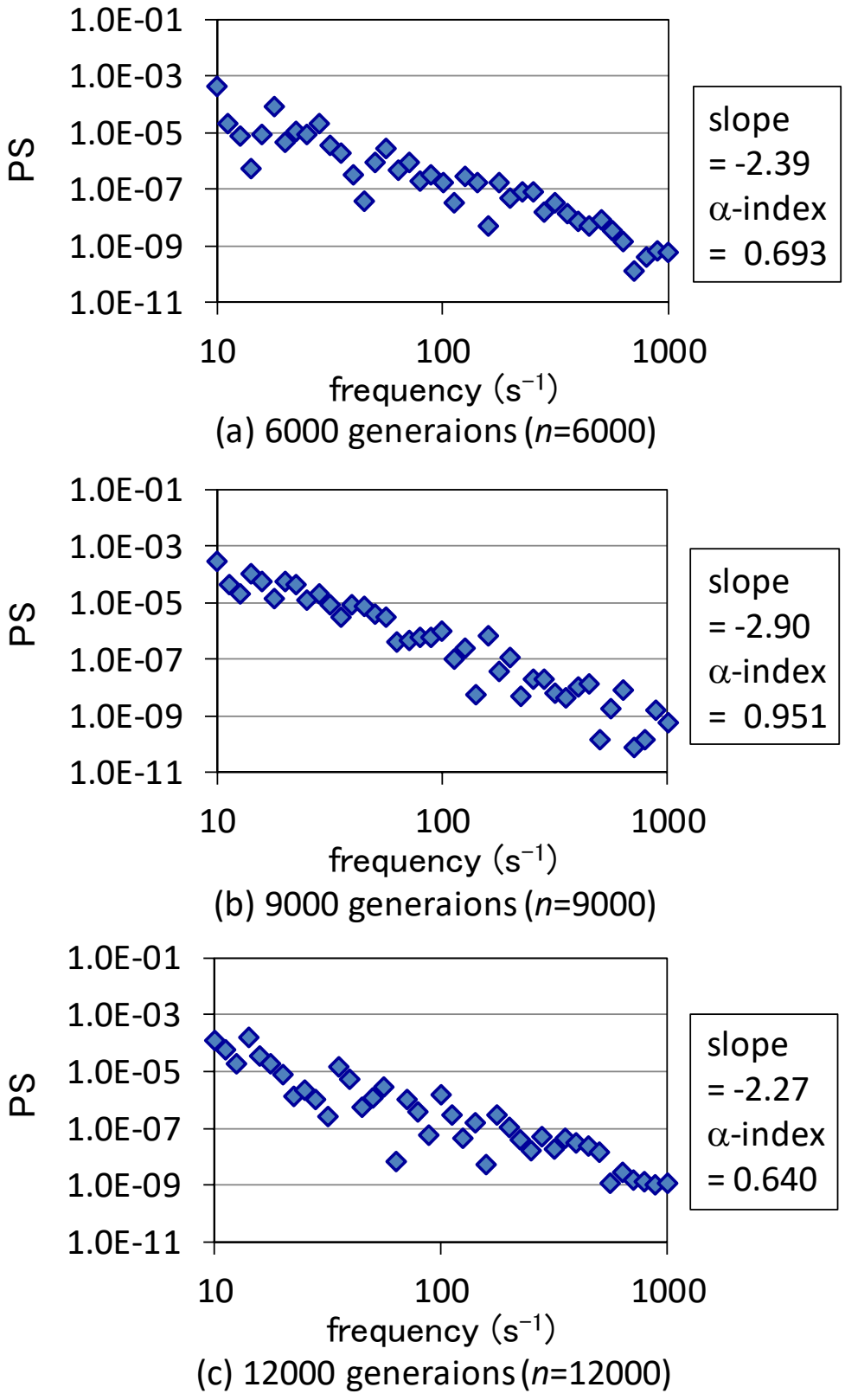

Figure 6. Power spectrum (PS) of replica i in Figure 4.

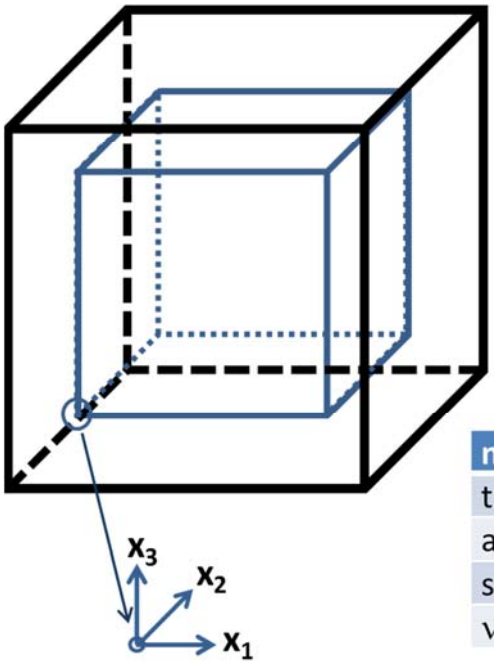

inside inner cube

- concrete
- burned fuel at 12GWd/t with fission products
- expected value of concrete volume fraction = 7/8

outside inner cube

concrete (100%)

one-group cross sections (cm^{-1})

material	fuel (F)	concrete (C)
total (Σ_T)	0.45324	0.47736
absorption(Σ_A)	0.07038	0.00159
scattering(Σ_S)	0.38286	0.47577
ν-fission($\nu\Sigma_F$)	0.09551	0.0

Figure 7. UO2-Concrete debris model.

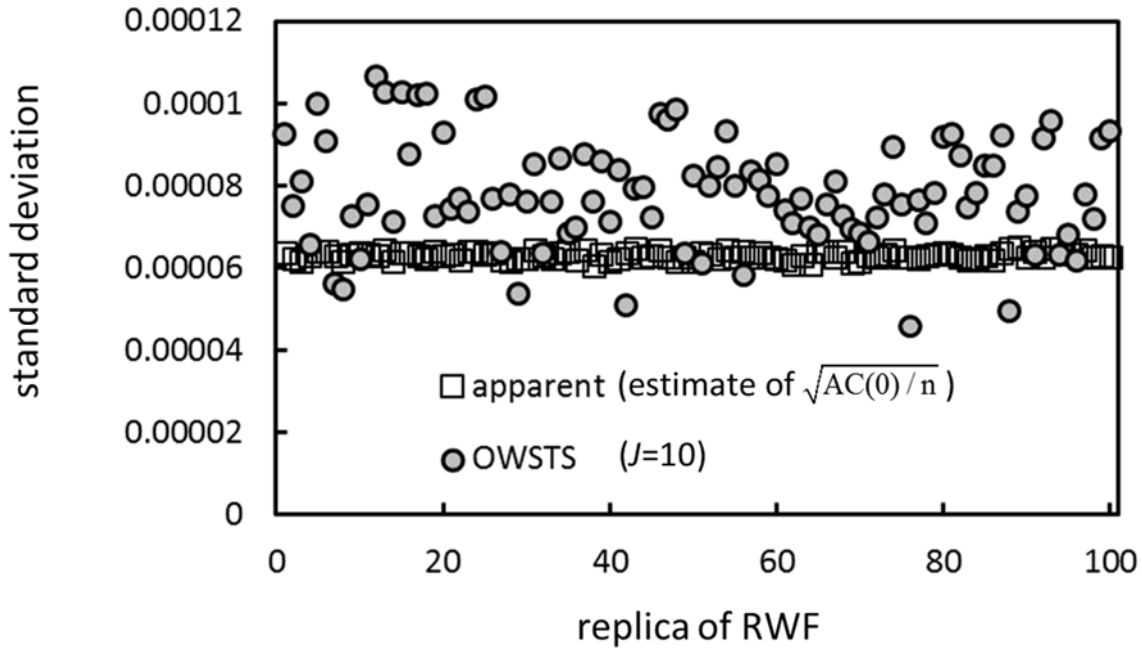

Figure 8. Standard deviation estimates of effective neutron multiplication factor (k_{eff}) of UO_2-concrete debris model; one whole set of MC criticality calculation consisting of 20000 particles per generation, 5000 generations and 1000 skip generations for each of 100 independent replicas of randomized Weierstrass function (RWF: α=0.5, λ=0.5, R=25cm); OWSTS for orthonormally weighted standardized time series estimates.

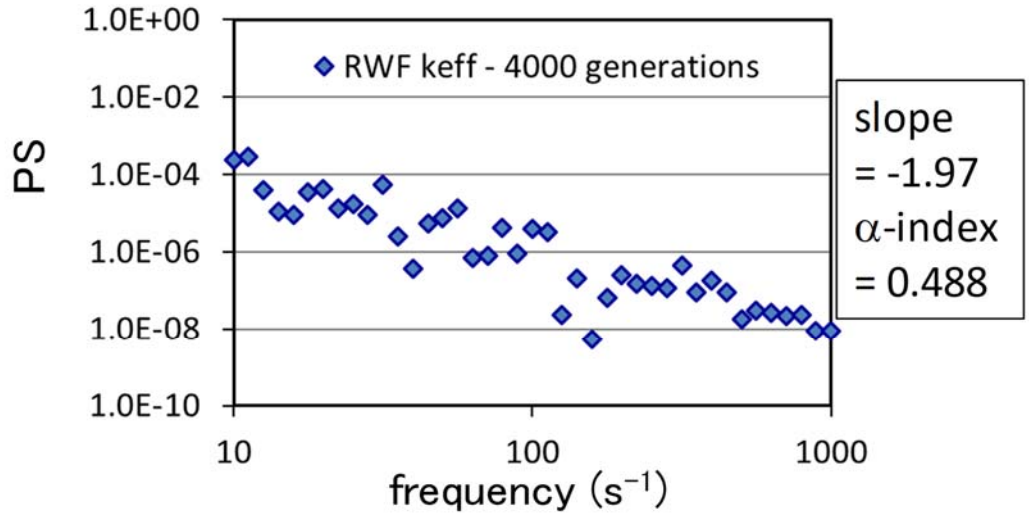

(a) Replica 12 – case of largest estimate of standard deviation in Figure 8

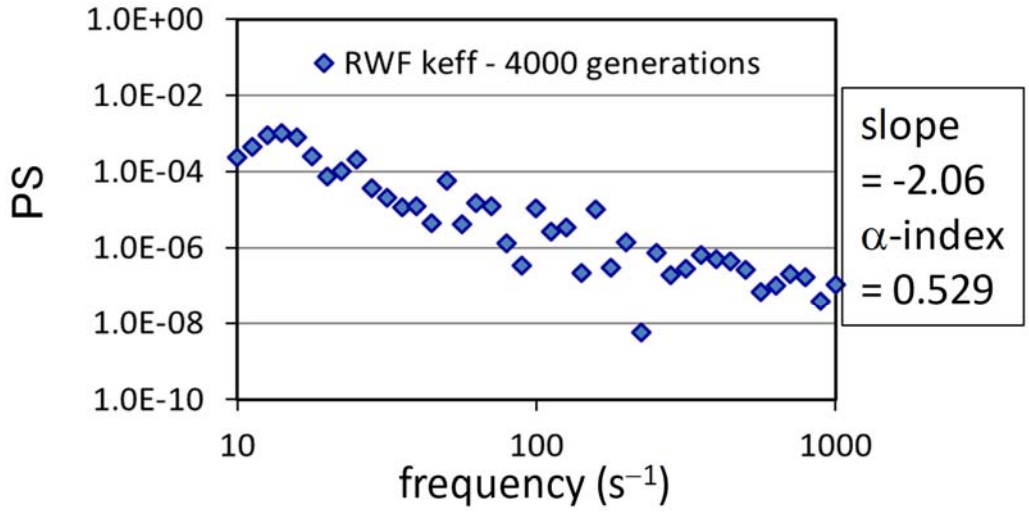

(b) Replica 76 – case of smallest estimate of standard deviation in Figure 8

Figure 9. Power spectrum (PS) of interpolated standardized time series of effective neutron multiplication factor (k_{eff}) in UO2-concrete debris model with randomized Weierstrass function (RWF).

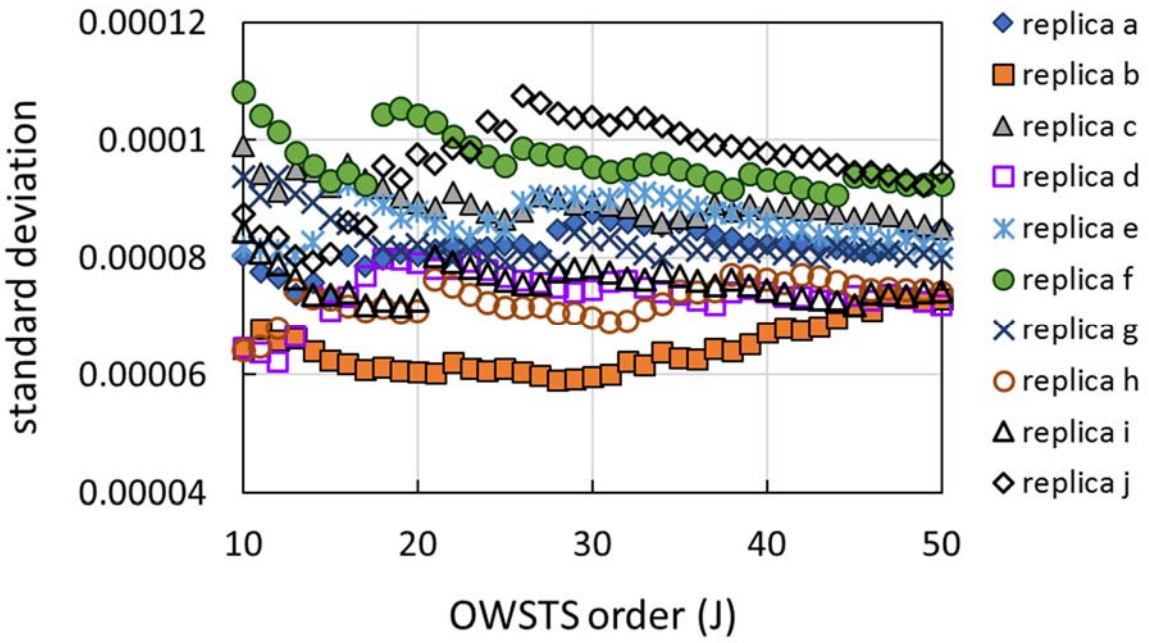

Figure 10. Converging behaviors of OWSTS standard deviation estimates of effective neutron multiplication factor of UO_2-concrete debris model; 10 independent realizations of randomized Weierstrass function (RWF: a=0.25, l=1.5, R=25) replicas; OWSTS for orthonormally weighted standardized time series estimates.